Ab initio second-harmonic susceptibilities of semiconductors: Generalized tetrahedron method and quasiparticle effects

B. Adolph and F. Bechstedt

Institut für Festkörpertheorie und Theoretische Optik, Friedrich-Schiller-Universität, D-07743 Jena, Germany

(Received 29 August 1997)

We report numerical calculations of the frequency-dependent second-order optical susceptibility. The results are based on an *ab initio* treatment of the geometry and the electronic structure within the density-functional theory in local-density approximation. The plane-wave-pseudopotential method is combined with a generalized tetrahedron method to perform the **k**-space integration. The analytic linear tetrahedron method has to be improved because of the energy-dependent prefactors of the δ functions describing the energy conservation. We also present results for spectra of the second-harmonic generation where many-body quasiparticle effects are included beyond the scissors-operator approximation. Zinc-blende semiconductors are considered as model substances. [S0163-1829(98)01911-0]

I. INTRODUCTION

In recent years, there has been an increasing interest in the nonlinear optical properties of various materials including zinc-blende semiconductors. This development is motivated by the rapid advances in electro-optical technology and all-optical information technology. One important nonlinear process is second-harmonic generation (SHG). Since its discovery in 1961,[1] technical difficulties delayed the accurate calculation of the corresponding susceptibility for many years. On the other hand, the microscopic understanding of the nonlinear processes is extremely important for the improvement of the nonlinear materials and devices and provides an opportunity to search for new materials.

Among the nonlinear-optical materials the III-V semiconductors InAs, GaAs, InP, and GaP are of central importance. They belong to the structurally simplest substances for which SHG is already allowed in the bulk. The optical nonlinearities are relatively large[2] and, moreover, can be increased if these materials are deposited in layered structures.[3] Other materials, like the group-IV compound SiC that also crystallizes in zinc-blende structure, show much lower nonlinearities.[4] It is important to know in which way slight changes in the electronic structure and the size of the atoms give rise to a remarkable variation of the nonlinear optical properties.

The calculation of the frequency-dependent linear or nonlinear optical properties of crystals requires the full information about its band structure and wave functions. Based on *ab initio* calculations the electronic structures of semiconductors have been available for several years. They have been used to describe the linear optical response from first principles.[5–9] In contrast, there are only few calculations of the same level of approximations in the case of the nonlinear response.[10–12] Huang and Ching[10] described the electronic structure of 15 semiconductors in the framework of the density-functional theory (DFT)[13] and the local-density approximation (LDA).[14] The wave functions have been expanded in terms of orthogonalized linear combinations of atomic orbitals (OLCAO). As in the linear case the **k** integration over the Brillouin zone (BZ) is performed using the ''traditional'' linear-analytic tetrahedron method according to Ref. 15. Levine[11] uses a plane-wave-pseudopotential code of the DFT-LDA. The special-points integration scheme requires a restriction to low frequencies. However, local-field and quasiparticle effects are also discussed. Hughes and Sipe[12] described the second-order optical response of the semiconductors GaAs and GaP using a combination of the full-potential linearized augmented plane-wave (FLAPW) method and DFT-LDA. Self-energy corrections are included on the level of the scissors-operator approximation. The **k**-space integration is performed by means of the traditional tetrahedron method in combination with a random sampling technique. The energies as well as the matrix elements are also linearized with respect to the **k** dependence.

The **k**-space integration in the nonlinear optical coefficients is more complicated than in the case of the linear response. Whereas the imaginary part of the linear optical susceptibility is mainly characterized by optical matrix elements multiplied with Dirac's δ function representing the energy conservation; rational functions of the optical transition energies involved in the nonlinear processes occur, in addition, in the case of the quadratic response. The **k** dependence of these functions remarkably influences the spectral behavior of the second-order susceptibilities. For that reason Moss, Sipe, and van Driel[16] extended the linear-analytic tetrahedron method for integrating linear-response functions to the nonlinear case. In addition, the linear variation of the two different optical transition energies appearing in the resonant prefactors due to the second-order nonlinear response have been taken into account. The electronic structures have been calculated within a tight-binding scheme.

In the present paper we combine this extended linear-analytic tetrahedron method with an electronic structure derived from an *ab initio* pseudopotential-plane-wave method. The advantage of the extension over the traditional tetrahedron method is shown. In addition, we discuss the effect of quasiparticle corrections on SHG spectra. The wave-vector- and band-index-dependent quasiparticle shifts are calculated from a slightly simplified expression for the exchange-

correlation self-energy. We investigate the prototypical III-V and IV-IV compound semiconductors GaP, GaAs, InP, InAs, and SiC crystallizing in zinc-blende structure. The paper is organized in the following way. In Sec. II we describe the computational method including the extension of the tetrahedron integration. Our results for the frequency-dependent SHG signals are presented in Sec. III and compared with other calculations and experimental data available. The effect of quasiparticle shifts deviating from the findings in the linear case and the convergence problems are discussed. A summary is given in Sec. IV.

II. COMPUTATIONAL METHOD

A. Second-harmonic coefficient

An expression for the second-order optical susceptibility $\hat{\chi}^{(2)}(\omega_1;\omega_2,\omega_3)$ is obtained from the quadratic-response theory.[17] One of the most important processes, the second-harmonic generation, is characterized by the tensor $\hat{\chi}^{(2)}(-2\omega;\omega,\omega)$ with ω as the frequency of the incident light. When the light-matter interaction is described by the coupling of the vector potential with the current density operator of the electrons, i.e., the so-called Coulomb or velocity gauge, the tensor is related to a correlation function of three current operators. In the single-particle picture the correlation function can be expressed in terms of Bloch eigenfunctions $|n\mathbf{k}\rangle$ belonging to the band index n, the wave vector $\mathbf{k}$ in the first Brillouin zone (BZ), and the Bloch energy $\varepsilon_n(\mathbf{k})$.[17,18] Excitonic and other effects beyond the

independent-particle approximation are neglected.[19] In $\hat{\chi}^{(2)}(-2\omega;\omega,\omega)$ occur only interband energies

$$E_{nn'}(\mathbf{k}) = \varepsilon_n(\mathbf{k}) - \varepsilon_{n'}(\mathbf{k}) \quad (1)$$

and matrix elements of the momentum operator

$$p_{nn'}^{\alpha}(\mathbf{k}) = \langle n\mathbf{k}|\mathbf{p}_\alpha|n'\mathbf{k}\rangle. \quad (2)$$

In general, the appearance of the momentum operator instead of the velocity operator indicates an approximation. Corrections due to spatially nonlocal potentials in the Schrödinger-like equation for the Bloch electrons and due to the incompleteness of the basis functions in the expansion of the Bloch functions[9] are neglected.

In the cubic case the tensor expression for $\hat{\chi}^{(2)}(-2\omega;\omega,\omega)$ may be remarkably simplified. Only the tensor components of the type $\chi_{xyz}^{(2)}(-2\omega;\omega,\omega)$ with x, y, and z as the cubic axes are different from zero. Only one function $\chi^{(2)}(\omega) \equiv \chi_{xyz}^{(2)}(-2\omega;\omega,\omega)$ has to be considered. Taking into account the time-reversal symmetry, it can be shown that the real and imaginary part of this function fulfil a Kramers-Kronig relation,[16] e.g.,

$$\text{Re } \chi^{(2)}(\omega) = \frac{2}{\pi}\int_0^\infty d\omega' \frac{\omega'}{\omega'^2 - \omega^2} \text{ Im } \chi^{(2)}(\omega'). \quad (3)$$

Following the derivation of Aspnes[18] the imaginary part is given by

$$\text{Im } \chi^{(2)}(\omega) = -\frac{\pi}{2}\left(\frac{e\hbar}{m}\right)^3 \frac{2}{V}\sum_{\mathbf{k}} \sum_{v,c,c'}{}' \{p_{vc}^x p_{cc'}^y p_{c'v}^z\}\left\{\frac{16}{E_{cv}^3(\mathbf{k})[2E_{c'v}(\mathbf{k}) - E_{cv}(\mathbf{k})]}\delta[E_{cv}(\mathbf{k}) - 2\hbar\omega]\right.$$
$$\left. + \frac{2E_{c'v}(\mathbf{k}) - E_{cv}(\mathbf{k})}{E_{cv}^3(\mathbf{k})[E_{cv}(\mathbf{k}) + E_{c'v}(\mathbf{k})][2E_{cv}(\mathbf{k}) - E_{c'v}(\mathbf{k})]}\delta[E_{cv}(\mathbf{k}) - \hbar\omega]\right\} \quad (4)$$

with

$$\{p_{vc}^x p_{cc'}^y p_{c'v}^z\} \equiv \text{Im}\left[\frac{1}{3!}\hat{P}(p_{vc}^x(\mathbf{k})p_{cc'}^y(\mathbf{k})p_{c'v}^z(\mathbf{k}))\right], \quad (5)$$

where $\hat{P}$ indicates all permutations with respect to the Cartesian components. V stands for the sample volume.

Expression (4) describes three-photon processes with the initial states of the electrons in an occupied valence band $n = v$ and the final states in an unoccupied conduction band $n = c$ or $n = c'$. Intermediate states may occur in valence as well as conduction bands. However, the virtual-hole contributions of a band combination $vv'c$ are found to be negligible[18] and are therefore omitted in Eq. (4). Only the virtual-electron contributions of the type $vc'c$ or vcc' are taken into account. Intraband processes do not play any role. Their vanishing may be shown using the time-reversal symmetry. Only terms, which fulfil the energy conservation for

positive frequencies, are written in expression (4) since only those frequencies are necessary in the Kramers-Kronig relation (3).

B. Brillouin-zone integration

In the explicit calculations we first calculate the imaginary part of the SHG susceptibility (4) in a wide range of frequencies. In a second step its real part is obtained by means of the Kramers-Kronig transformation (3). The introduction of the permutations of the Cartesian coordinates in Eq. (5) corresponds to the construction of an invariant against all point group operations. Together with the time-reversal symmetry such invariants allow the restriction of the BZ integration to the irreducible part, i.e., a $\frac{1}{48}$th wedge of the BZ of the fcc structure.

The appearance of Dirac's δ functions in expression (4) is a consequence of the energy conservation during the SHG process. These functions indicate that the $\mathbf{k}$-space integration should be performed by means of the linear-analytic tetrahe-

dron method[15,20] as well known from the linear optical properties. The prefactors of the δ functions are replaced by the average over the four corners of a tetrahedron. However, the situation is more complicated in the case of the nonlinear optics. Besides momentum matrix elements the prefactors contain energy denominators and nominators. Consequently, in expression (4) for the imaginary part of the SHG susceptibility ''double resonances'' may occur. In both contributions, the 2ω and the ω term, this coincidence happens when $2\hbar\omega = E_{cv}(\mathbf{k})$ and $\hbar\omega = E_{c'v}(\mathbf{k})$ ($c \neq c'$).

Because of the possibility of double resonances the variation of the prefactors of the δ functions cannot be ignored. This can be only done in the case of the momentum matrix elements to a good approximation. The $\mathbf{k}$ variation of the interband energies has to be taken into account, at least also in a linear approximation. The details of this integration are described in Ref. 16 The basic idea is to replace the $\mathbf{k}$-space integral over a tetrahedron by a finite energy integral over the fraction of the isoenergy face lying within the tetrahedron. This isoenergy face is defined by the transition energy, which governs the δ function. Because of the occurrence of two different optical transition energies due to the second-order nonlinear process, a second integration has to be analytically performed. It gives the length of a line segment. It is defined as the intersection of the isoenergy plane related to the second interband energy in the prefactor with the plane of intersection defined by the δ function. In analogy to the linear case, the line segment may be written in terms of the known energies at the tetrahedron vertices.

There are limits that require special care. As in the linear case, if the energies at the vertices of the tetrahedron become degenerate, one must analytically calculate the area of intersection to avoid large numerical errors. In the nonlinear case there are also complications when the interband energies $E_{cv}(\mathbf{k})$ and $E_{c'v}(\mathbf{k})$ are parallel in $\mathbf{k}$ space. This case may be formally treated by using the formula in Eq. (4) and performing the BZ integration over the δ functions as in the linear case.

C. Structure, electronic states, and quasiparticle shifts

The electronic-structure calculations underlying the computations of the SHG susceptibility are based on the DFT-LDA.[21] The many-body electron-electron interaction is described within the Ceperley-Alder scheme[22] as parametrized by Perdew and Zunger.[23] The electron-ion interaction is treated by norm-conserving, *ab initio*, fully separable pseudopotentials in the Kleinman-Bylander form.[24] They are based on relativistic all-electron calculations for the free atoms by solving the Dirac equation self-consistently. In the beginning the pseudopotentials were generated according the Bachelet-Hamann-Schlüter scheme.[25] The carbon potential is softened by carefully choosing the core radii.[26]

The electronic wave functions are expanded in terms of plane waves. The energy cutoffs for the plane-wave expansion are chosen to 15 Ry for the III-V compounds and 34 Ry in the case of silicon carbide (SiC). They are sufficient for converged energy and lattice calculations. The total-energy optimizations within the zinc-blende structure give rise to theoretical cubic lattice constants of $a = 5.36$ Å (GaP), 5.57 Å (GaAs), 5.67 Å (InP), 5.86 Å (InAs), and 4.29 Å (SiC).

They are used although they slightly underestimate the experimental values[27] and, hence, enlarge somewhat the DFT-LDA transition energies. These transition energies are calculated according to Eq. (1). The single-particle energies $\varepsilon_n(\mathbf{k})$ are replaced by the eigenvalues of the Kohn-Sham equation.

In order to account for the excitation aspect, exchange and correlation have to be treated more carefully. At least quasiparticle (QP) shifts $\Delta_n(\mathbf{k})$, which account for the differences between the exchange-correlation self-energy and the corresponding potential used in the DFT-LDA,[28,29] have to be taken into consideration. The QP corrections to the DFT-LDA eigenvalues are computed within the *GW* approximation,[28,29] according to a slightly simplified scheme developed by Cappellini and co-workers.[30,31] We determine such band-index- and wave-vector-dependent QP shifts explicitly and discuss their influence in detail for zinc-blende SiC.[32] In addition we compare the results including QP shifts within the *GW* approximation with those using a scissors-operator approximation as suggested in Ref. 12. In the case of the III-V compounds we restrict ourselves to the scissors-operator approximation. The scissors operators are determined from the comparison of calculated and measured linear optical spectra.

We know already from the treatment of the linear optical properties that the inclusion of the QP effects requires physical considerations[9] and cannot be restricted to a replacement of all transition energies in Eq. (4) by differences of $\varepsilon_n(\mathbf{k}) + \Delta_n(\mathbf{k})$. When QP effects are included, the spatial nonlocality of the self-energy influences the optical transition operator in the same manner as other nonlocal potential contributions. However, we neglect this influence. Another problem arises from the fact that only the single-particle energies in expression (4) which are introduced from the spectral properties should be shifted. In the linear case this problem is now solved[6,9,33] within the assumption of nearly equal DFT-LDA and QP wave functions. Which energies should be shifted is related to a derivation of the optical susceptibility starting from a longitudinal (scalar) perturbation. In the electric-dipole approximation and neglecting nonlocal contributions one uses the relation

$$p_{nn'}^{\alpha}(\mathbf{k}) = i\frac{m}{\hbar}[\varepsilon_n(\mathbf{k}) - \varepsilon_{n'}(\mathbf{k})]\langle n\mathbf{k}|x_\alpha|n'\mathbf{k}\rangle \qquad (6)$$

to avoid ill-defined matrix elements of the dipole operator. The energies arising from this rewriting should not be corrected by QP effects. Consequently, because of the three matrix elements of the momentum operator in Eq. (4), we introduce a renormalization factor $[\varepsilon_n(\mathbf{k}) + \Delta_n(\mathbf{k}) - \varepsilon_{n'}(\mathbf{k}) - \Delta_{n'}(\mathbf{k})]/[\varepsilon_n(\mathbf{k}) - \varepsilon_{n'}(\mathbf{k})]$ for each of the matrix elements in expression (4). The renormalization factor increases the oscillator strengths according to the increase of the gaps. There are further complications due to the screening dynamics included in the QP self-energy. For a discussion of the dynamical effects the reader is referred to Ref. 34.

III. RESULTS AND DISCUSSION

A. BZ sampling

From the calculation of the linear optical properties we know that in the zinc-blende case about 30 bands are suffi-
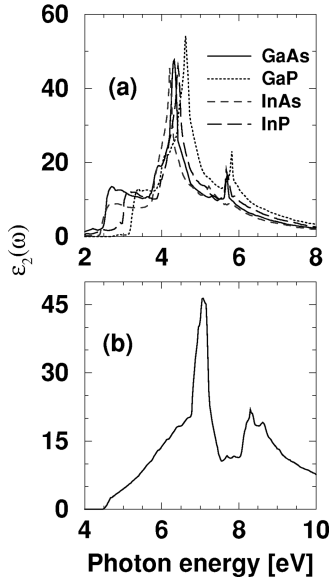
FIG. 1. Imaginary part of the dielectric function for III-V compounds (a) and cubic SiC (b) calculated with 505 **k** points in the linear tetrahedron method.

cient for a converged calculation of the imaginary part of the optical susceptibility.[9] The real part calculated via the Kramers-Kronig transformation does not show significant changes after increasing the number of bands. Therefore, we restrict ourselves in the calculation of the SHG coefficient to 24 bands (without spin), four valence bands, and the first 20 conduction bands. However, we increase the number of **k** points and, hence, the number of tetrahedrons. Whereas in the linear case reasonable results may be obtained with 89 **k** points,[9] in the nonlinear case the mesh should be finer because of prefactors in expression (4). Figure 1 shows the linear results obtained with 505 mesh points for GaP, GaAs, InP, InAs, and SiC. In the SiC case the effect of the increase of the **k**-point density is weak. The low-energy peak with E_0 and E_1 character as well as the high-energy peak with E_1', E_0', and $E_2 + \delta$ character are hardly influenced, where we follow the denotations of Yu and Cardona.[35] The effect is larger in the case of the low-energy E_1 peak in the spectra of the III-V compounds. Because of the nearly parallel empty and occupied bands, the increase of the density in the **k**-point mesh gives rise to a more pronounced E_1 peak. The intensity of the E_2 structure is slightly reduced. Its shoulder is related to E_0' transitions. The E_1' peak higher in energy is hardly influenced by the sampling.

Figure 2 represents two effects, the dependence of the SHG spectra on the density of the **k** points in the sampling and the comparison of the analytic linear tetrahedron method[15,20] with its generalization for nonlinear optical coefficients[16] described in Sec. II B. The principal behavior and the most important peak structures appear already for 89 **k** points. This is related to the fact that the general behavior of Im $\chi^{(2)}(\omega)$ is already given by the combined density of states and the optical matrix elements. However, there is also an influence of the energy denominators in the prefactors of the 2ω and ω terms. In the case of the generalized tetrahedron method one observes an increasing number of fine structures. Their physical relevance is low. After introduction of lifetime broadening effects by a Lorentz convolution
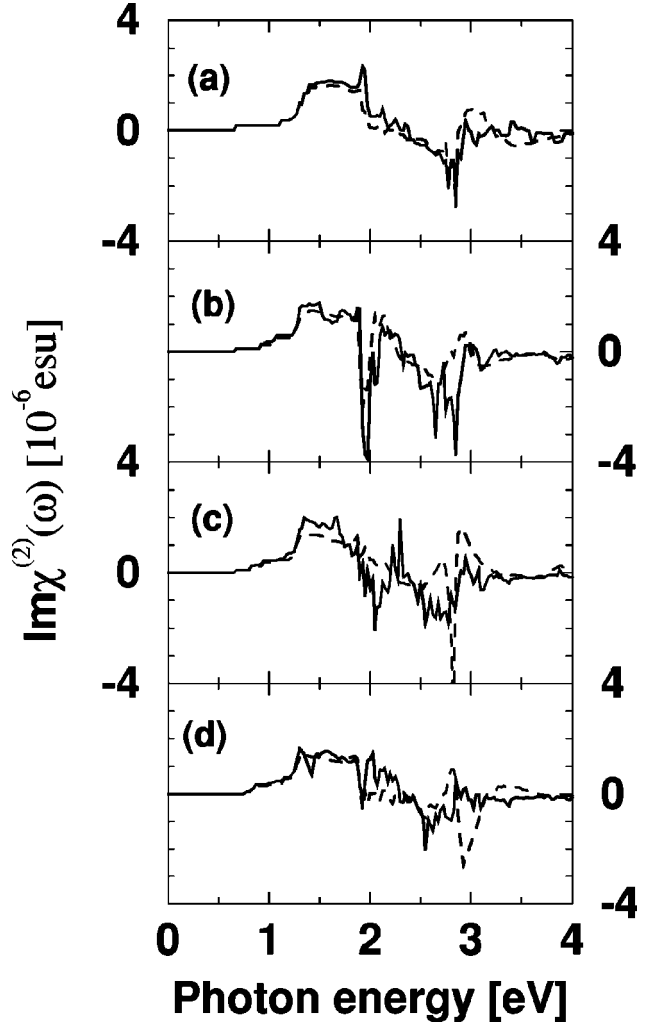

FIG. 2. Imaginary part of the second-order susceptibility Im $\chi^{(2)}(\omega)$ of GaAs for different numbers $N_\mathbf{k}$ of **k** points. (a) $N_\mathbf{k}$ = 89, (b) $N_\mathbf{k}$ = 240, (c) $N_\mathbf{k}$ = 505, and (d) $N_\mathbf{k}$ = 916. Solid line, tetrahedron method as in the linear case; dashed line, generalized tetrahedron method.

these structures disappear widely. The spike structures in the spectra calculated using the common linear tetrahedron method fluctuate with the **k**-point sampling. This indicates their unphysical nature. Rather, they are related to the previously mentioned double resonances, which should be avoided by the described generalization of the method. Figure 2 shows two conclusions: (i) The density of the used

TABLE I. Convergence of $\chi^{(2)}(0)$ of GaAs in units of 10^{-8} esu with the number of **k** points $N_\mathbf{k}$, for two different numbers of bands, 8 and 24. The values are calculated by means of the Kramers-Kronig relation (3) and by a direct calculation after performing the Kramers-Kronig integral by using Dirac's δ functions (values in parentheses).

Bands	$N_\mathbf{k}$=89	$N_\mathbf{k}$=240	$N_\mathbf{k}$=505	$N_\mathbf{k}$=916
8	30	15	22	31
	(37)	(39)	(40)	(38)
24	47	22	30	39
	(44)	(47)	(48)	(46)

TABLE II. Low-frequency SHG coefficients $\chi^{(2)}(0)$ (in 10^{-8} esu) calculated by two different methods for III-V compounds. They are compared with results from other calculations (Refs. 10, 12, 16, and 18) or measurements (Refs. 2, 39, and 40).

Reference	GaP	GaAs	InP	InAs
Present	15	30	14	32
	(16)	(48)	(17)	(35)
12	13	23		
10	32	60	28	174
16	38	96		450
18	24	38		64
39	52	90		200
40	20	43		
2	32	91	69	

k-point meshes should be increased in the nonlinear case with respect to the sampling used for linear optical coefficients. In the following we use 505 **k** points in the irreducible part of the fcc BZ. (ii) When the whole SHG spectrum is calculated from the imaginary part and the Kramers-Kronig transformation, the analytic linear tetrahedron method has to be improved. Therefore, all of the following spectra are computed using 505 **k** points.

For two different numbers of bands, 8 and 24, the convergence of the zero-frequency SHG coefficient is shown in Table I with respect to the number of **k** points. The values for $\chi^{(2)}(0)$ obtained from a direct **k**-space integration, where the Kramers-Kronig transformation is analytically performed by using Dirac's δ functions in the imaginary part, are already converged for 89 mesh points. The nonmonotonous variation of the values derived from the Kramers-Kronig analysis indicates the need of more **k** points in this type of integration. In contrast to other zinc-blende materials GaAs seems to be an exceptional case with respect to the convergence of the SHG coefficient calculated by means of the
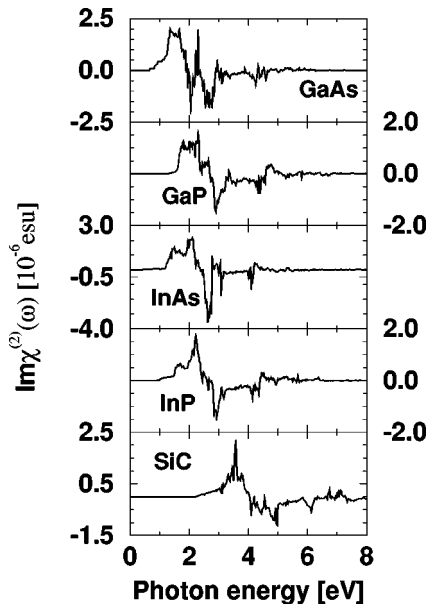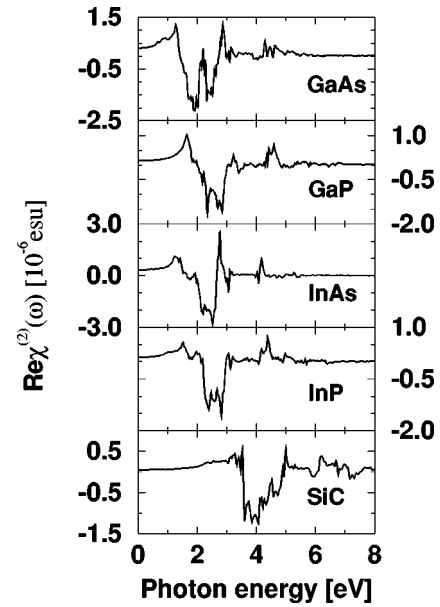

FIG. 4. Real part of $\chi^{(2)}(\omega)$ for five different materials crystallizing in zinc-blende structure. 505 **k** points and 24 bands have been used in the calculation.

FIG. 3. Imaginary part of $\chi^{(2)}(\omega)$ for five different materials crystallizing in zinc-blende structure. 505 **k** points and 24 bands have been used in the calculation.
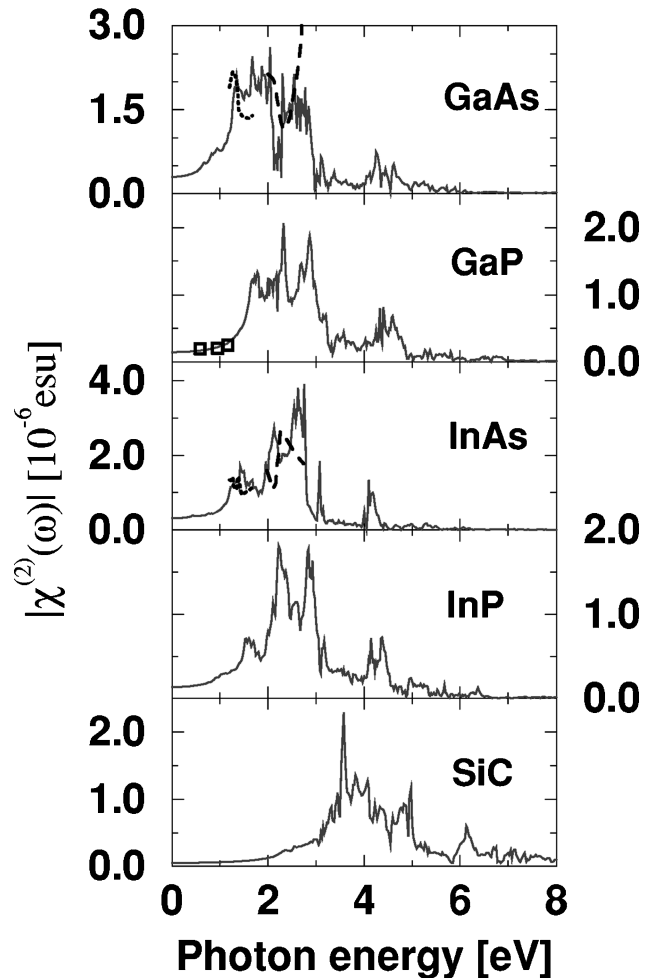

FIG. 5. Module of $\chi^{(2)}(\omega)$ for five different materials crystallizing in zinc-blende structure. 505 **k** points and 24 bands have been used in the calculation. Experimental data are also shown. GaP: Ref. 36. GaAs: dotted (Ref. 37), dashed (Ref. 38). InAs: dotted (Ref. 37), dashed (Ref. 38).

Kramers-Kronig transformation. This is related to the band structure. There are band pairs and BZ regions where similar shapes exist, reducing the convergence as also seen from Fig. 2. That means that a tendency already known for the E_1 region in the linear spectra is much more pronounced in the nonlinear case.

B. Spectral behavior of SHG coefficients

The SHG coefficients for GaP, GaAs, InP, InAs, and SiC are plotted in Figs. 3, 4, and 5. Figures 3 and 4 show the imaginary and real part, respectively. The module of the total coefficient is plotted in Fig. 5. The calculations are performed using 505 **k** points and 24 bands. In Fig. 5 also experimental data[36–38] are shown for comparison. The prominent structures in all spectra are limited to a region of 5 (7) eV for the III-V compounds (SiC). That means that the fact that $\chi^{(2)}(\omega)$ is related to three optical transitions and that only the imaginary part of the product of the three matrix elements occurs has remarkable consequences.

The simplified picture of superposing two combined density of states at 2ω and ω according to the contributions to Eq. (4) is not valid. First, the 2ω term dominates the SHG coefficient. Second, the spectral behavior of Im $\chi^{(2)}(\omega)$ (Fig. 3) can be explained by the two promined categories of optical transitions, E_1 and E_2, in the linear absorption of, at least, the III-V compounds. However, matrix-element effects are much stronger in the nonlinear case. In comparison to the linear absorption the peaks are sharpened and the sign could be negative in accordance to the prefactor. The sign of the imaginary part of the product of three momentum matrix elements is not fixed.

Since the spectra for the four III-V compounds are very similar, we discuss Im $\chi^{(2)}(\omega)$ (cf. Fig. 3) in more detail only for GaAs taking the transition energies from the DFT-LDA calculation. In the 2ω contribution a pronounced positive E_1 peak appears at $2\hbar\omega \approx 2.7$ eV. In the same frequency region a smaller E_0 peak related to the ω contribution is observed near $\hbar\omega \approx 1.4$ eV. The E_2 peak in the 2ω term possesses a negative sign. It occurs around $2\hbar\omega \approx 4.4$ eV. A similar behavior follows for the E_1' peak at about $2\hbar\omega = 5.6$ eV. In the ω contribution to the imaginary part one finds weaker E_1 and E_2 peaks at $\hbar\omega$ with an opposite sign. Their peak positions follow from the linear absorption spectra plotted in Fig. 1. The corresponding values for InAs (InP,GaP) are 2.6 (3.1,3.4) eV for E_1, 4.2 (4.5,4.6) for E_2, and 5.2 (5.7,5.8) eV for E_1'. The situation is more complicated in the case of cubic SiC. The low-energy peak with E_0 and E_1 character and the high-energy peak with E_1', E_0', and $E_2 + \delta$ character, which occur near energies $\hbar\omega = 7.0$ eV and 8.4 eV in the linear absorption spectrum, appear both in the 2ω and the ω contribution. Thereby the high-energy peak changes the sign as already discussed for the III-V semiconductors.

The interpretation of the real parts (Fig. 4) of the SHG coefficients is more complicated than those of the Im $\chi^{(2)}(\omega)$ spectra. However, according to the Kramers-Kronig transformation the spectra are smoother and look like the superposition of the spectra of more or less four pronounced oscillator spectra with resonance frequencies close to the E_1- and E_2-like structures appearing in the 2ω and ω
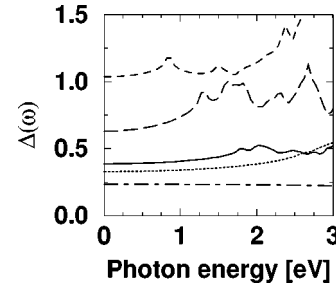

FIG. 6. Check of Miller's rule for InAs, GaAs, InP, GaP, and SiC in decreasing order.

terms of the imaginary parts.

The comparison of the module of the total SHG coefficients with experimental data[36–38] for GaP, GaAs, and InAs (Fig. 5) indicates a reasonable description of the SHG spectra by the presented theory. This holds especially for the order of magnitude and the principal spectral behavior. In the case of GaAs there are also certain indications that the peak observed for photon energies around 1.3 eV by Parson and Chang[37] may be interpreted mainly by optical transitions along the ΓL line near Γ in the BZ.

C. Low-frequency limit

The corresponding spectra are already plotted in Figs. 4 and 5. From these figures we derive the values 0.15 (GaP), 0.30 (GaAs), 0.14 (InP), and 0.32 (InAs) 10^{-6} esu for $\chi^{(2)}(0)$. Because of the strong frequency variation of the imaginary part including positive and negative contributions the accuracy of the obtained values is limited. In the Kramers-Kronig transformation the calculation of the exact spectral weights of these positive and negative peaks is very important. They cancel each other partially during the integration. More exact values follow when the Kramers-Kronig integral is analytically performed by means of Dirac's δ functions in Im $\chi^{(2)}(\omega)$ in Eq. (4) and the **k**-space integration is done directly. The values resulting for 505 mesh points and 24 bands are 0.16 (GaP), 0.48 (GaAs), 0.17 (InP), and 0.35 (InAs) 10^{-6} esu.

In Table II the values calculated for III-V compounds are compared with results of other calculations and measurements. In the limit $\omega \rightarrow 0$ the SHG coefficients $\chi^{(2)}(0)$ also describe the electro-optic susceptibility. There are remarkable fluctuations in the values. However, considering the different methods and approximations used and the difficulties in the measurements, we state a reasonable overall agreement. Only in the case of InAs are the discrepancies really large.

We have seen from the peak structure in the spectra that are some similarities with those known from the linear optics. For that reason Miller[41] suggested that the SHG susceptibility $\chi^{(2)}(\omega)$ of a crystal should be related to the linear susceptibility $\chi^{(1)}(\omega)$ by

$$\Delta(\omega) = \chi^{(2)}(2\omega)/\{\chi^{(1)}(2\omega)[\chi^{(1)}(\omega)]^2\}. \quad (7)$$

The function $\Delta(\omega)$ is expected to be a slowly varying function of ω. $\Delta(0)$ should be a certain universal constant. The function $\Delta(\omega)$ is plotted in Fig. 6 versus photon energies below the important resonances for several III-V semiconductors and zinc-blende SiC. There is a clear chemical trend with the lattice constant of the considered materials. $\Delta(\omega)$
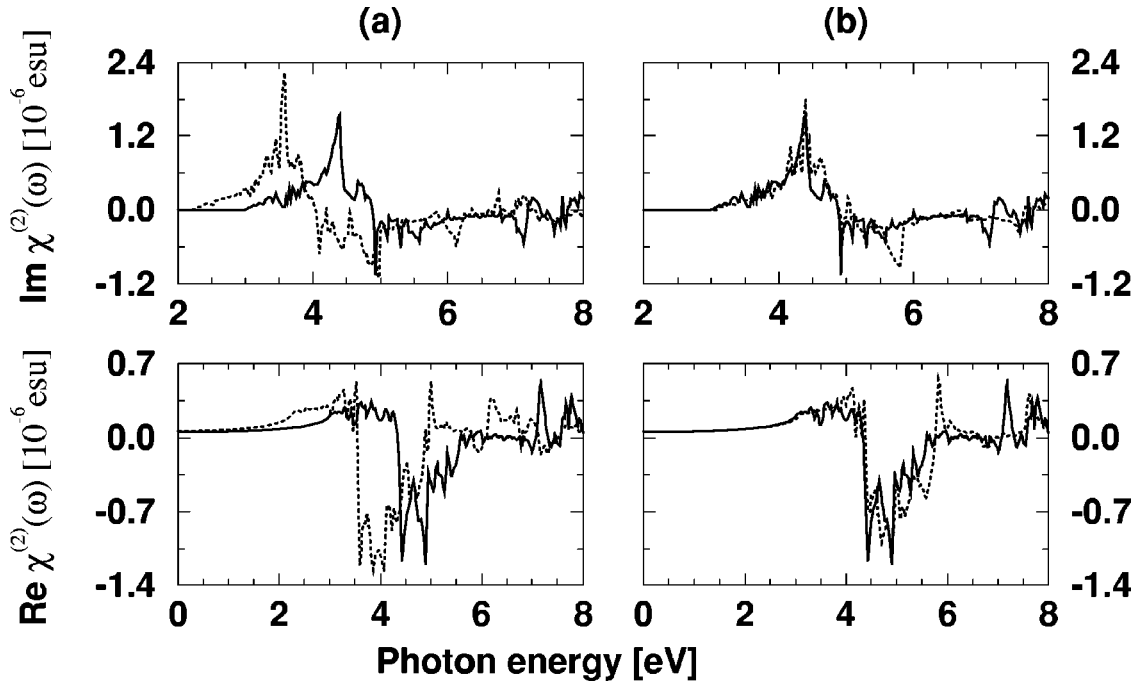
FIG. 7. Influence of quasiparticle corrections: imaginary and real part of the SHG coefficient for SiC. (a) Results within DFT-LDA (dotted line) and within the *GW* approximation (solid line), (b) results within the *GW* approximation (solid line) and using a scissors operator (dotted line).

decreases with the lattice constant. Such a decrease seems to be a general tendency for wide-gap materials with small lattice constant and a remarkable ionic contribution to the chemical bond.[42] The corresponding bond-charge model seems to be also able to explain the chemical trend in $\chi^{(2)}(0)$ values and even the sign change for compounds containing first-row elements by ionicity of chemical bonds and atomic sizes. In the case of compounds like GaAs with nearly equally sized atoms the ''covalent'' contribution to $\chi^{(2)}(0)$ vanishes. Only the ''ionic'' contribution determines the value of $\chi^{(2)}(0)$. With increasing difference in the size of the atoms, especially when elements like C or N are present, the ''covalent'' contribution will be important. Since its sign is reversed, the total quantity is remarkably lowered or even the sign of the SHG coefficient could be changed in certain wide-gap semiconductors. In any case, the values $|\chi^{(2)}(0)|$ are smaller than for conventional III-V semiconductors.

D. Quasiparticle effect

The influence of QP effects within the *GW* approximation on the SHG intensity is shown in Fig. 7(a) for SiC. On a first view, there seems to be the main influence similar to the situation in the linear optical case.[9] Despite the inclusion of the band-index and wave-vector dependence of the QP shifts, $\Delta_n(\mathbf{k})$, the spectra are more or less rigidly shifted towards higher photon energies. The shift of the main peaks in the low-energy region of Im $\chi^{(2)}(\omega)$ amounts to 0.84 eV. This value is exactly half the one derived in the linear case[9] for the main absorption peak with E_1', E_0', and $E_2' + \delta$ character. This indicates again that the main peaks in the low-frequency region are related to the 2ω contributions. In the high-frequency region the interpretation of DFT-LDA and the QP spectrum is more complicated because of the superposition of 2ω and ω contributions. In comparison with measured

SHG coefficients we expect another complication. We know that such QP shifts somewhat overestimate the opening of optical gaps. Smaller values of the many-body shifts are necessary,[9] due to the presence of excitonic effects.

In Fig. 7(b) the influence of the QP corrections on the SHG spectra is compared for two different approximations, on the one hand the scissors-operator approximation, and on the other hand, the full *GW* approximation discussed in Fig. 7(a), i.e., taking into account wave-vector- and band-index-dependent shifts. The value used for the scissors operator is not uniquely defined. We assume a rigid shift of the excitation energies of 1.68 eV, which corresponds to the energetical distance of the main 2ω contributions in DFT-LDA and full QP approximation in Fig. 7(a). The difference between the two approximations of the QP effects can be clearly seen from the comparison of the main peaks around 4.5 eV. We find the spectra within the *GW* approximation to contain less pronounced structures in comparison with the ones calculated using the scissors operator. The wave-vector- and band-index-dependent QP shifts seem to cause a smoothing of the structures and a partial annihilation of the contributions of the 2ω and ω term as a result of the complicated structure of the energy denominators in the prefactors, whereas the rigid shift within the scissors-operator approximation does not. This happens especially in the energy region above the main peak. The situation in the high-energy region is somewhat confusing due to the simultaneous occurrence of 2ω and ω contributions. Due to the use of one rigid shift the partial compensation of the two different types of contributions is different. For that reason, pronounced structures appear around 6 and 7 eV in one spectrum but not in the other one.

Our observation holds not only for the imaginary part but also for the real part. In the spectral region above the half of the energy of the main absorption peaks, the scissors-operator approximation is less successful than in the case of

the linear optical spectra. In the region below the main structures the spectra are only influenced by the sensitivity of the prefactors to the actual transition energies resulting in small variations of the graph. The discrepancy between the two QP approximations practically vanishes for zero frequency. The value of the second-order nonlinear coefficient changes from 6.2×10^{-8} esu, as for the result of the DFT-LDA to 5.3×10^{-8} esu (5.4×10^{-8} esu), taking into account QP corrections within the GW (scissors-operator) approximation.

IV. SUMMARY

We have studied the influence of two different types of tetrahedron methods to perform the **k**-space integration over Dirac's δ functions in the imaginary part of the second-order optical susceptibility. We found that because of their strong energy dependence the prefactors of the δ functions have to be properly treated. This is in contrast to the linear case where the prefactors are only governed by optical transition matrix elements. Moreover, for the same reason it turns out that the density of the **k**-point mesh has to be increased with respect to the linear findings.

The mains structures in the SHG spectra may be explained by the same optical transitions that already govern the linear optical properties. In the case of the III-V compounds they are transitions of the types E_1 and E_2. However, matrix elements are more important than in the linear case. They are able to change the sign of a certain contribution that is related to pronounced optical transitions. The main features observed in the experimental SHG spectra available seem to be described by the presented theory. Describing the low-frequency SHG coefficient, the **k** integration has to be performed more carefully to account for the partial cancellation of the 2ω and ω contributions in the second-order susceptibility. The resulting values $\chi^{(2)}(0)$ approach the calculated and measured data in the average. Miller's rule is not fulfilled with a universal constant. Rather, there is a clear chemical trend in the values for several compounds.

In order to include also the excitation aspect in the electronic band structure usually described within DFT-LDA, we have also taken into account wave-vector- and band-index-dependent quasiparticle corrections. Because of the energy-dependent prefactors of Dirac's δ functions in the imaginary part of the SHG susceptibility, the quasiparticle effects give rise to spectral changes that cannot be discussed within a simplified picture of a scissors operator.

[1] P. A. Franken, A. E. Hill, C. W. Peters, and G. Weinreich, Phys. Rev. Lett. **7**, 118 (1961).

[2] S. Singh, in *Handbook of Laser Science and Technology*, edited by M. J. Weber (CRC, Cleveland, 1986), Vol. III, Pt. 1, p. 88.

[3] P. Boucard, F. H. Julien, D. D. Yang, J.-M. Lourtioz, E. Rosencher, and P. Bois, Opt. Lett. **16**, 199 (1991).

[4] S. Singh, J. R. Potopowicz, L. G. Van Uitert, and S. H. Wemple, Appl. Phys. Lett. **19**, 53 (1971).

[5] M. Alouani, L. Brey, and N. N. Christensen, Phys. Rev. B **37**, 1167 (1988).

[6] Z. H. Levine and D. C. Allan, Phys. Rev. Lett. **63**, 1719 (1989); Phys. Rev. B **43**, 4187 (1991).

[7] B. Engel and B. Farid, Phys. Rev. B **46**, 15 812 (1992).

[8] M.-Z. Huang and W. Y. Ching, Phys. Rev. B **47**, 9464 (1993).

[9] B. Adolph, V. I. Gavrilenko, K. Tenelsen, F. Bechstedt, and R. Del Sole, Phys. Rev. B **53**, 9797 (1996).

[10] M.-Z. Huang and W. Y. Ching, Phys. Rev. B **45**, 8738 (1992); **47**, 9464 (1993).

[11] Z. H. Levine, Phys. Rev. B **49**, 4532 (1994).

[12] J. L. P. Hughes and J. E. Sipe, Phys. Rev. B **53**, 10 751 (1996).

[13] P. Hohenberg and W. Kohn, Phys. Rev. **136**, B864 (1964).

[14] W. Kohn and L. J. Sham, Phys. Rev. **140**, A1133 (1965).

[15] G. Lehmann and M. Taut, Phys. Status Solidi B **119**, 9 (1983).

[16] D. J. Moss, J. E. Sipe, and H. M. van Driel, Phys. Rev. B **36**, 1153 (1987); **36**, 9708 (1987).

[17] P. N. Butcher and T. P. McLean, Proc. Phys. Soc. London **81**, 219 (1963); **83**, 579 (1964).

[18] D. E. Aspnes, Phys. Rev. B **6**, 4648 (1972).

[19] V. I. Gavrilenko and F. Bechstedt, Phys. Rev. B **55**, 4343 (1997).

[20] D. Jespen and O. K. Anderson, Solid State Commun. **9**, 1763 (1971).

[21] R. Stumpf and M. Scheffler, Comput. Phys. Commun. **79**, 447 (1994).

[22] D. M. Ceperley and B. I. Alder, Phys. Rev. Lett. **45**, 566 (1980).

[23] J. P. Perdew and A. Zunger, Phys. Rev. B **23**, 5048 (1981).

[24] L. Kleinman and D. M. Bylander, Phys. Rev. Lett. **48**, 1425 (1982).

[25] G. B. Bachelet, D. R. Hamann, and M. Schlüter, Phys. Rev. B **26**, 4199 (1982).

[26] P. Käckell, B. Wenzien, and F. Bechstedt, Phys. Rev. B **50**, 17 037 (1994).

[27] *Physics of Group IV Elements and III-V Compounds*, edited by O. Madelung, Landolt-Börnstein, New Series, Group III, Vol. 17, Pt. a (Springer, Berlin, 1982).

[28] M. S. Hybertsen and S. G. Louie, Phys. Rev. B **34**, 5390 (1986).

[29] F. Bechstedt, Adv. Solid State Phys. **32**, 161 (1992).

[30] G. Cappellini, R. Del Sole, L. Reining, and F. Bechstedt, Phys. Rev. B **47**, 9892 (1993).

[31] B. Wenzien, G. Cappellini, and F. Bechstedt, Phys. Rev. B **51**, 14 701 (1995).

[32] B. Wenzien, P. Käckell, F. Bechstedt, and G. Cappellini, Phys. Rev. B **52**, 10 897 (1995).

[33] R. Del Sole and R. Girlanda, Phys. Rev. B **48**, 11 789 (1993).

[34] F. Bechstedt, K. Tenelsen, B. Adolph, and R. Del Sole, Phys. Rev. Lett. **78**, 1528 (1997).

[35] P. Y. Yu and M. Cardona, *Fundamentals of Semiconductors* (Springer, Berlin, 1996).

[36] M. M. Choy and R. L. Byer, Phys. Rev. B **14**, 1693 (1976).

[37] F. G. Parson and R. K. Chang, Opt. Commun. **3**, 173 (1971).

[38] D. Bethune, A. J. Schmidt, and Y. R. Shen, Phys. Rev. B **11**, 3867 (1975).

[39] J. J. Wynne and N. Bloembergen, Phys. Rev. **188**, 1211 (1969).

[40] B. F. Levine and C. G. Bethea, Appl. Phys. Lett. **20**, 272 (1972).

[41] R. C. Miller, Appl. Phys. Lett. **5**, 17 (1964).

[42] B. F. Levine, Phys. Rev. Lett. **25**, 440 (1970).